Brownian Dynamics of Sterically-Stabilized Colloidal Suspensions

Ward E. TeGrotenhuis, Clayton J. Radke, and Morton M. Denn
Center for Advanced Materials, Lawrence Berkeley Laboratory and
Dept. of Chemical Engineering, University of California, Berkeley, CA 94720

Using Brownian dynamics, equilibrium and dynamic properties are calculated for colloidal suspensions that are stabilized through the Milner, Witten and Cates (1988) steric potential. Results are reported for osmotic pressures, radial distribution functions, static structure factors, and self-diffusion coefficients. The sterically-stabilized systems are also approximated by equivalent hard spheres, with good agreement for osmotic pressure and long-range structure. The suitability of the potential to model the behavior of a real system is explored by comparing static structure factors calculated from Brownian dynamics simulations to those measured using SANS (Markovic et al., 1986). Finally, the effects of Hamaker and hydrodynamic forces on calculated properties are investigated.

Introduction

Detailed knowledge of the microstructure of colloidal suspensions is necessary for comprehensive understanding of macroscopic behavior, including both equilibrium and transport properties. One application where microstructure plays a critical role is in the production of specialty ceramics, where colloidal suspensions act as precursors; here the microstructure influences the structural, thermal, optical and electrical properties of the ceramic products.

In this work, Brownian dynamics is used to calculate equilibrium macroscopic properties, equilibrium microstructure, and diffusion coefficients of sterically-stabilized colloidal suspensions of monodisperse, spherical particles. Brownian dynamics is a tool for simulating the equilibrium and nonequilibrium behavior of suspensions from first principles, allowing for the averaging of solvent forces. For a given interparticle potential, the simulation gives exact results for calculated properties within the statistical uncertainty of the computations (and, of course, the physical assumptions implicit in the formulation). This attribute provides a bridge between theory and experimental measurement.

Steric interactions are short range, typically extending only to distances on the order of the particle size; they are incorporated here through an interparticle potential developed by Milner, Witten, and Cates (MWC) (1988) for systems with strongly-stretched terminally-attached polymers. Other interparticle forces, such as Hamaker attractive forces (Hamaker, 1984) and hydrodynamic interactions, can also be important; they are included in several simulations for comparison.

The theory of hard spheres provides a frame of reference for interpreting and evaluating the behavior observed in sterically stabilized suspensions. Brownian dynamics calculations are compared to experimentally-measured static structure factors of a sterically-stabilized colloidal system obtained from small-angle neutron scattering (SANS) experiments by Markovic and coworkers (1986). The equivalent hard-sphere calculations prove useful in evaluating the differences between the SANS experiments and the simulations.

Background

Brownian dynamics

Brownian dynamics employs the Langevin equation (Langevin, 1908; Chandrasekhar, 1943; Ermak and McCammon, 1978) as the equation of motion for suspended particles. Including hydrodynamic and direct interactions, the N-particle Langevin equation written in vector notation is

$$m \cdot \frac{dv}{dt} = -R \cdot v + F + A(t) \tag{1}$$

Equation 1 describes $3N$ force balances and $3N$ torque balances

W. E. TeGrotenhuis is currently with Batelle PNL, Richland, WA 99352.

for an N-particle system. $\boldsymbol{m}$ is the inertial tensor, $\boldsymbol{v}$ is a $6N$ vector of translational and angular velocities of the particles, t is time, $\boldsymbol{R}$ is the $6N \times 6N$ resistance matrix (Brenner, 1964), and $\boldsymbol{F}$ is a vector of net direct forces on the particles. $\boldsymbol{A}$ represents random fluctuating forces and torques due to collisions with molecules in the suspending medium, with the following statistical properties:

$$\langle \boldsymbol{A}(t) \rangle = 0 \tag{2a}$$

$$\langle \boldsymbol{A}(0)\boldsymbol{A}(t) \rangle = 2kT\boldsymbol{R}\delta(t) \tag{2b}$$

Here k is Boltzmann's constant, T is absolute temperature, and $\delta(t)$ is the Dirac delta function. Equations 2a and 2b were obtained by Deutch and Oppenheim (1971) through a statistical mechanical approach; they may also be derived from the fluctuation-dissipation theorem (Bossis et al., 1982; Ciccotti and Ryckaert, 1981; van Gunsteren and Berendsen, 1982).

The first term on the right side of Eq. 1 arises because of hydrodynamic forces on the particles. The resistance matrix, $\boldsymbol{R}$, which is a function only of configuration for spherical particles (Brenner, 1964), can be written as a combination of Stokes drag, written as

$$\boldsymbol{R}_\infty = \frac{kT}{D_o}\boldsymbol{I} \tag{3}$$

and a term accounting for interactions between the particles. $\boldsymbol{I}$ is the identity matrix, and D_o is the free-diffusion coefficient. Only Stokes drag remains in the limit of infinite dilution. Setting $\boldsymbol{R} = \boldsymbol{R}_\infty$ in Eqs. 1 and 2 decouples the force equations from the torque equations, eliminating the need to solve the latter. This simplification is used in the simulations when calculating only equilibrium properties, because they are unaffected by hydrodynamic interactions. When hydrodynamic interactions between the particles are included, particle rotation is assumed to be minimal, because the systems are quiescent and the particles experience no direct torques. Thus, the hydrodynamic coupling between rotation and translation is ignored, and only the $3N$ force equations are required.

Calculation of hydrodynamic interactions is based on a pairwise additive approximation for hard spheres developed by Durlofsky et al. (1987) which captures both long-range, multibody interactions and short-range lubrication forces. Details of the adaptation for the absence of force-torque coupling and an analysis of the error in the approximation are described in TeGrotenhuis (1990).

The second term on the right side of Eq. 1 represents the net direct force on the particles, which includes direct forces between the particles and body forces; the latter are neglected in this work. Pairwise additivity of the interparticle forces is assumed, so the net force on particle i is

$$\boldsymbol{F}_i = \sum_j -\frac{dU(r_{ij})}{dr}\frac{\boldsymbol{r}_{ij}}{r_{ij}} \tag{4}$$

where the sum is over the other particles; $U(r)$ is the potential of interaction between two particles with centers separated by distance r.

Solutions to Eq. 1 are obtained using a numerical method developed by Ermak and McCammon (1978), which is accurate to $O(\Delta t)$, where Δt is the integration time step. Details are given in TeGrotenhuis (1990). Simulations are carried out in dimensionless form, and all reported parameters and calculated properties are nondimensionalized using the characteristic dimensions in Table 1.

Table 1. Characteristic Dimensions Used for Nondimensionalization

Length scale	a	particle radius
Energy	kT	temperature times Boltzmann's constant
Time	$\frac{a^2}{D_o} = \frac{6\pi\mu a^3}{kT}$	characteristic time for free diffusion

Interaction potential

The Milner, Witten and Cates interaction potential (1988; Milner, 1988) is obtained from a self-consistent field approach to the free energy of strongly-stretched, terminally-attached polymers, corresponding to moderate surface coverage. The authors applied this expression for the free energy to the situation of two identical flat plates separated by a distance s. The polymers are assumed not to interdigitate and are compressed by the second plate to a height of one-half the plate separation. With the Derjaguin approximation (Derjaguin, 1934), the following dimensionless interaction energy between two spheres of radius a is obtained:

$$U_s(s) = C_o h_o \left[\ln\left(\frac{h_o}{s}\right) + \frac{9}{5}\left(\frac{s}{h_o}\right) - \frac{1}{3}\left(\frac{s}{h_o}\right)^3 + \frac{1}{30}\left(\frac{s}{h_o}\right)^6 - \frac{3}{2} \right]$$

when

$$s < h_o \tag{5}$$

The energy of interaction is zero when $s > h_o$, where s is the dimensionless separation distance of the particle surfaces. The equilibrium height of the chains is h^*, which appears in Eq. 5 as $h_o = 2h^*/a$. C_o is defined as

$$C_o \equiv 2\pi a^2 \sigma N_f \left(\frac{\sigma w}{\alpha}\right)^{2/3} (\pi^2/96)^{1/3} \tag{6}$$

where N_f is the polymerization index of the equivalent freely-jointed chain, σ is the surface coverage in number of chains per unit area, and w is the excluded volume parameter (de Gennes, 1979) defined as

$$w = \alpha^3(1 - 2\chi) \tag{7}$$

Here, α is the size of a monomer of an equivalent freely-jointed chain, and χ is the Flory interaction parameter.

Hamaker (1937) forces are included in several simulations for comparison. The potential of interaction used in Eq. 4 for these simulations is

$$U(r) = U_s(r-2) + U_H(r) \tag{8}$$

where

$$U_H(r) = -\frac{A}{3}\left[\frac{4\left(1-\frac{2}{r^2}\right)}{r^2-4} + \ln\left(1-\frac{4}{r^2}\right)\right] \tag{9}$$

This model is simplistic, because it does not account for the presence of the stabilizer layer. Nevertheless, it is adequate to explore possible effects of Hamaker attractive forces.

Simulations

All simulations are performed at constant temperature, volume and number of particles in a cubic box of edge length L_b (nondimensionalized by particle radius). The number density and volume fraction are, respectively,

$$N_p = \frac{N}{L_b^3} \tag{10}$$

$$\phi = \frac{4\pi}{3}\frac{N}{L_b^3} \tag{11}$$

The particle concentration is fixed for a given number of particles (N) by setting the box edge length (L_b), the number density (N_p), or the volume fraction (ϕ). Periodic boundary conditions with the nearest-neighbor convention (Allen and Tildesley, 1987) are used to eliminate wall effects. Pairwise hydrodynamic interactions are spherically truncated at a distance equal to half the box size, L_b. Simulations are conducted using 108 and 256 particles. Preliminary simulations were performed to allow the system to 'heat up' from a state of lower configurational energy to equilibrium at the desired conditions, and the final configurations were subsequently used as initial configurations for simulations used to calculate properties. Random Brownian displacements are generated using a pseudo-random number generator; details are in TeGrotenhuis (1990).

Properties

Calculated properties include the radial distribution function, the static structure factor, the osmotic pressure, and the self-diffusion coefficient. The radial distribution is calculated by (Allen and Tildesley, 1987)

$$g(r) = \frac{1}{N_p N}\left\langle \sum_{i=1}^{N}\sum_{j\neq i=1}^{N} \delta(r - r_{ij}) \right\rangle \tag{12}$$

where r_{ij} is the vector from the center of particle i to the center of particle j, and the brackets denote the ensemble average. In calculating the radial distribution function, the domain of r is discretized into segments, an average value of $g(r)$ is computed for each segment, and the value is assigned to the midpoint of the interval. The nearest-neighbor convention restricts the domain of the computed $g(r)$ to be less than or equal to one-half the box length.

Spatial correlations in the number density in Fourier space are captured in the static structure factor, which is related to the radial distribution function through the equation (Chandler, 1987)

$$S(K) = 1 + 4\pi N_p \int_0^\infty r^2[g(r) - 1]\frac{\sin(Kr)}{Kr}\,dr \tag{13}$$

Equation 13 is used to obtain $S(K)$ from the calculated $g(r)$ through a fast Fourier transform (FFT) (Press et al., 1986). The calculated radial distribution function is extrapolated beyond the truncation point by setting $g(r) = 1$ to meet the FFT requirement for 2^n evenly-spaced function values, where n is an integer.

The virial theorem (Hirschfelder et al., 1954) is used to compute the osmotic pressure of a suspension from periodically-sampled particle configurations. With pairwise-additive forces and periodic boundary conditions, the osmotic pressure is calculated as (Dickinson, 1983)

$$\frac{P}{N_p} = 1 + \frac{1}{3N}\left\langle \sum_{i=1}^{N}\sum_{j=i+1}^{N} \boldsymbol{r}_{ij}\cdot\boldsymbol{F}_{ij} \right\rangle \tag{14}$$

$\boldsymbol{F}_{ij}$ is the pair force between particles i and j and has the same direction as $\boldsymbol{r}_{ij}$.

The self-diffusion coefficient was determined from the slope of the mean-square displacement (MSD) curve (Chandler, 1987; Dickinson, 1983)

$$D_s(t) \equiv \frac{1}{6}\frac{d}{dt}\langle |\boldsymbol{r}_j(t) - \boldsymbol{r}_j(0)|^2 \rangle \tag{15}$$

where D_s is nondimensionalized by the free-diffusion coefficient. The focus here is to obtain the long-time self-diffusion coefficient, $D_{s,L}$, defined as:

$$D_{s,L} = \lim_{t\to\infty} D_s(t) \tag{16}$$

The mean-square displacement curve is extended to several characteristic times, and an average slope of the upper part is computed using linear regression. The average indicated by the angular brackets in Eq. 15 is computed by averaging over many starting times, t^o, and over all particles in the system (Marqusee and Deutch, 1980). The N_o starting times are separated by m time steps. The average mean-square displacement at a discrete value of time is therefore calculated as

$$\langle [\Delta r(t)]^2 \rangle = \frac{1}{N_o N}\sum_{j=1}^{N_o}\sum_{i=1}^{N} |\boldsymbol{r}_i(t + t_j^o) - \boldsymbol{r}_i(t_j^o)|^2 \tag{17}$$

Equivalent hard spheres

The systems of particles interacting through the MWC potential were also approximated by an equivalent hard-sphere system. The only parameter in the hard-sphere potential is the size of the particles, which is characterized by the hard-sphere radius, a_{hs}. The other parameter needed to specify the thermodynamic state is the volume fraction or, equivalently, the particle number density. Barker and Henderson (1967) defined the equivalent hard-sphere radius for a potential $U(r)$ as

$$a_{hs} = \frac{1}{2}\int_0^\infty \{1 - \exp[-U(r)]\}\,dr \tag{18}$$

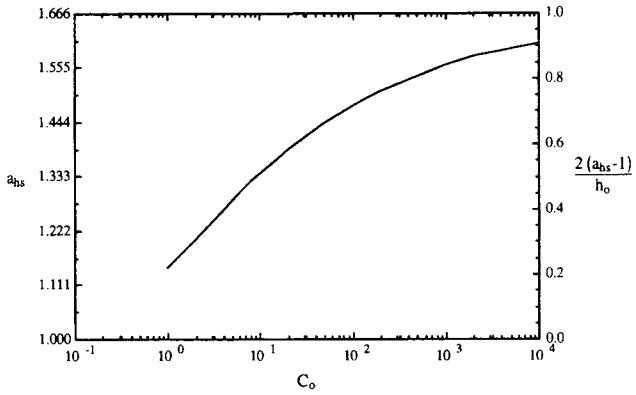

Figure 1. Equivalent hard-sphere radius for the MWC potential as a function of the magnitude parameter C_o for $h_o = 1.333$.

The MWC potential diverges to infinity at $r = 2$, so there is an implied hard-core region of $r \leq 2$, where the potential is infinite. Figure 1 illustrates how the equivalent hard-sphere radius for the MWC potential with $h_o = 1.333$ changes as the magnitude parameter C_o increases. Even when $C_o = 10^4$, the steric potential shows a small degree of softness. The scale on the right side of Figure 1 normalizes the equivalent hard-sphere radius by the sum of the core particle radius and the equilibrium stabilizer thickness. When $2(a_{hs} - 1)/h_o = 1$, the stabilizer layer is solid and cannot be penetrated. The equivalent hard-sphere volume fraction is calculated as

$$\phi_{hs} = \phi (a_{hs})^3 \tag{19}$$

where ϕ is the volume fraction of the hard core of the sterically-stabilized particle.

The osmotic pressure of hard-sphere systems can be obtained from the Carnahan-Starling equation of state (Carnahan and Starling, 1970) as follows:

$$\frac{P_{CS}}{N_p} = \frac{1 + \phi_{hs} + \phi_{hs}^2 - \phi_{hs}^3}{(1 - \phi_{hs})^3} \tag{20}$$

Employing the equivalent hard-sphere volume fraction calculated from Eq. 19, an equivalent hard-sphere pressure is obtained from Eq. 20, which is thus compared to the osmotic pressure calculated from the Brownian dynamics simulations.

Perram's algorithm (Perram, 1975), which solves the Percus-Yevick integral equations (Percus and Yevick, 1958), generates $g(r)$ curves for hard-sphere systems at specific volume fractions, and comparisons of results to the exact solutions of the Percus-Yevick equations obtained by Throop and Bearman (1965) verify agreement to at least three significant digits at the volume fractions used in this article. Static structure factors are calculated for the hard-sphere systems using Fourier transforms as described above. The hard-sphere structure factors are clearly inaccurate near $K = 0$ [$S(0) < 0$ is physically impossible], probably because of truncation of $g(r)$ or inaccuracies in the Percus-Yevick approximation at low wave number (Barker and Henderson, 1972), but the results are relevant in the region of the first peak of $S(K)$ and to the right.

Table 2. Parameters and Prior Runtime at the Same Conditions (t_e) for Brownian Dynamics Simulations

Case	C_o	h_o	ϕ	N_c	Δt	t_e
A	4.0	1.333	0.2238	20,000	0.00005	1.0
B	20.0	1.333	0.0850	20,000	0.0005	5.0
C	20.0	1.333	0.1000	20,000	0.0005	5.0
D	20.0	1.333	0.1300	20,000	0.0005	5.0
E	20.0	1.333	0.1493	20,000	0.00005	0.5
F	1.0	1.333	0.1493	20,000	0.00005	0.5
G	2.0	1.333	0.1493	20,000	0.00005	1.5
H	5.0	1.333	0.1493	20,000	0.00005	1.5
I	10.0	1.333	0.1493	20,000	0.00005	0.5
J	2.0	1.20	0.1493	20,000	0.00005	0.5
K	2.0	1.00	0.1493	20,000	0.00005	0.5

Comparison to Equivalent Hard Spheres

Parameters for the Brownian dynamics simulations are compiled in Table 2. The steric interactions are characterized by the potential parameters C_o and h_o, and the particle concentration is indicated by the volume fraction of core particles ϕ. The number and size of the time steps (N_c and Δt, respectively) are given, as well as the number of dimensionless time units t_e that were run at the same conditions in previous simulations to allow the system to relax to equilibrium.

The equivalent hard-sphere radius, volume fraction, and osmotic pressure for the systems in Table 2 are given in Table 3. During the Brownian dynamics simulations, osmotic pressures were calculated at each time step, and the averages are shown in the fifth column of Table 3. Estimates of 68% confidence intervals of the calculated pressure are also reported. Approximation by the osmotic pressure of the equivalent hard-sphere system improves with increasing C_o and decreasing h_o, because the MWC potential becomes steeper and shorter range, respectively. Particle concentration also becomes increasingly important as the equivalent hard-sphere system approaches the hard-sphere phase transition, which occurs at about 51% (Barker and Henderson, 1972); this is demonstrated most graphically by the poor agreement for case A.

Figure 2 shows a series of radial distribution functions calculated with fixed potential parameters at decreasing volume fractions. Radial distribution functions for the equivalent hard spheres are also shown, all of which have the same equivalent hard-sphere radius. Both radial distribution functions display

Table 3. Equivalent Hard-Sphere Radii, Volume Fractions, and Osmotic Pressures for Brownian Dynamics Simulations, with Osmotic Pressures and 68% Confidence Limits Calculated from Brownian Dynamics Simulations

Case	a_{hs}	ϕ_{hs}	P_{CS}/N_p	P/N_p	Error Estimate
A	1.2647	0.4528	9.5524	7.8342	±0.0910
B	1.3872	0.2269	2.7417	2.7098	±0.0359
C	1.3872	0.2670	3.3493	3.2655	±0.0375
D	1.3872	0.3471	5.1217	4.8901	±0.0488
E	1.3872	0.3985	6.8633	6.1451	±0.2327
F	1.1463	0.2248	2.7133	2.7044	±0.2811
G	1.2048	0.2610	3.2497	3.0390	±0.0625
H	1.2834	0.3155	4.3137	4.1413	±0.0607
I	1.3383	0.3577	5.4348	5.0873	±0.1393
J	1.1761	0.2428	2.9657	2.8816	±0.1255
K	1.1350	0.2182	2.6277	2.6338	±0.2120

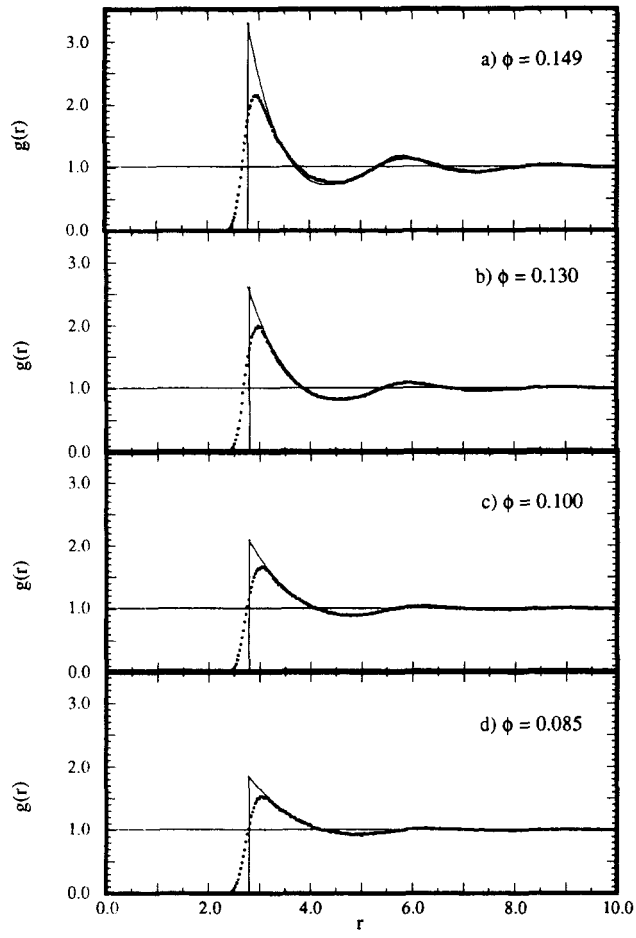

Figure 2. Radial distribution functions calculated for $C_o = 20.0$ and $h_o = 1.333$ at the indicated volume fractions, from Brownian dynamics results (■ ■ ■) and for equivalent hard-sphere systems (——).

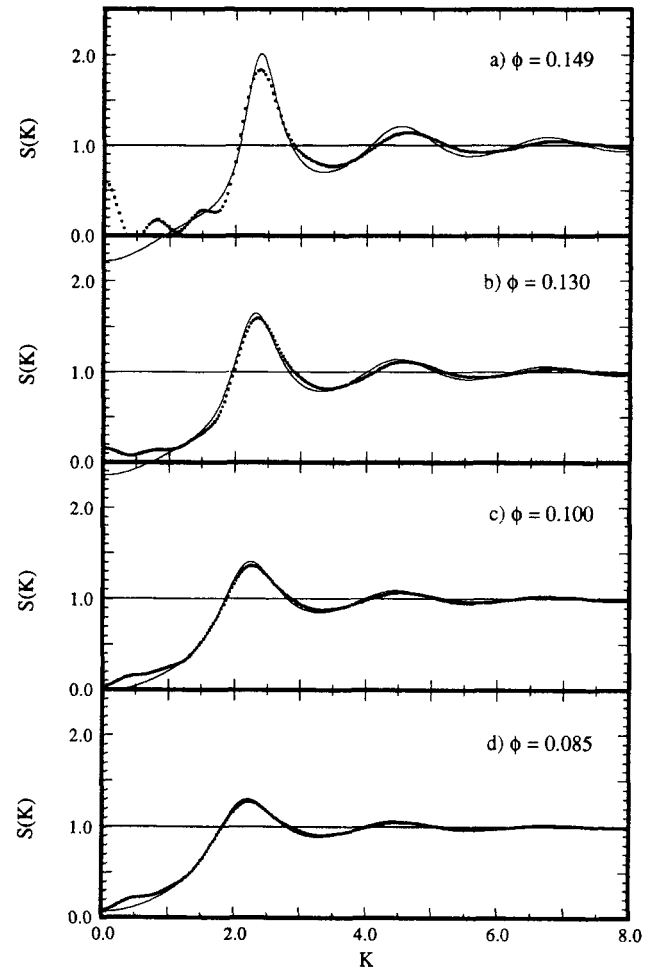

Figure 3. Static structure factors calculated for $C_o = 20.0$ and $h_o = 1.333$ at the indicated volume fractions, from Brownian dynamics results (■ ■ ■) and for equivalent hard-sphere systems (——).

appreciable structure at the highest volume fraction (Figure 2a); two peaks and possibly a third are discernible. The steric potential is soft enough to permit penetration of the equivalent hard-sphere diameter, resulting in a lower, broader primary peak in the steric system to the right of the hard-sphere peak. Agreement between the radial distribution functions improves as r increases, but slight discrepancies are visible at the first minimum and the second peak, with the hard-sphere peak being closer to the central particle. As the volume fraction decreases (Figures 2b-2d), the structure in both curves decreases, the long-range agreement between the curves improves, and the steric system continues to have a lower, broader primary peak. Whereas the hard-sphere peak does not shift with volume fraction, the primary peak of the steric system slowly shifts to the right as the volume fraction decreases.

The static structure factors obtained from the curves in Figure 2 are displayed in Figure 3. There is less agreement in Fourier space between the equivalent hard-sphere and steric $S(K)$ curves, but the agreement improves at lower volume fractions, and the peak positions coincide closely at all concentrations; both peaks shift to the left as volume fraction decreases.

Figure 4 demonstrates how $S(K)$ changes as the potential parameter C_o is decreased while keeping h_o and ϕ constant. As the interactions diminish, the equivalent hard-sphere radius and concentration decrease, causing the primary $S(K)$ peak for the hard spheres and for the steric system to shift to the right and the structure (peak heights) to diminish. The peak heights are overpredicted by the equivalent hard-sphere system owing to the softness of the steric potential, but the peak positions coincide closely.

Sensitivity of the microstructure to changes in h_o is shown in Figure 5. The hard-sphere radius and the structure are relatively insensitive to h_o in the range of h_o values investigated. A 30% change in h_o results in relatively small changes in the peak heights and peak positions in both the equivalent hard-sphere and steric curves.

In general, the MWC potential is well characterized over a wide parameter range by the equivalent hard-sphere system. Macroscopic properties such as the osmotic pressure are estimated closely, and the long-range microstructure exhibited by $g(r)$ at large r is approximated very well far from the hard-sphere phase transition. The short-range structure is not described by the equivalent hard-sphere system because of the softness of the potential. The most noticeable feature in the

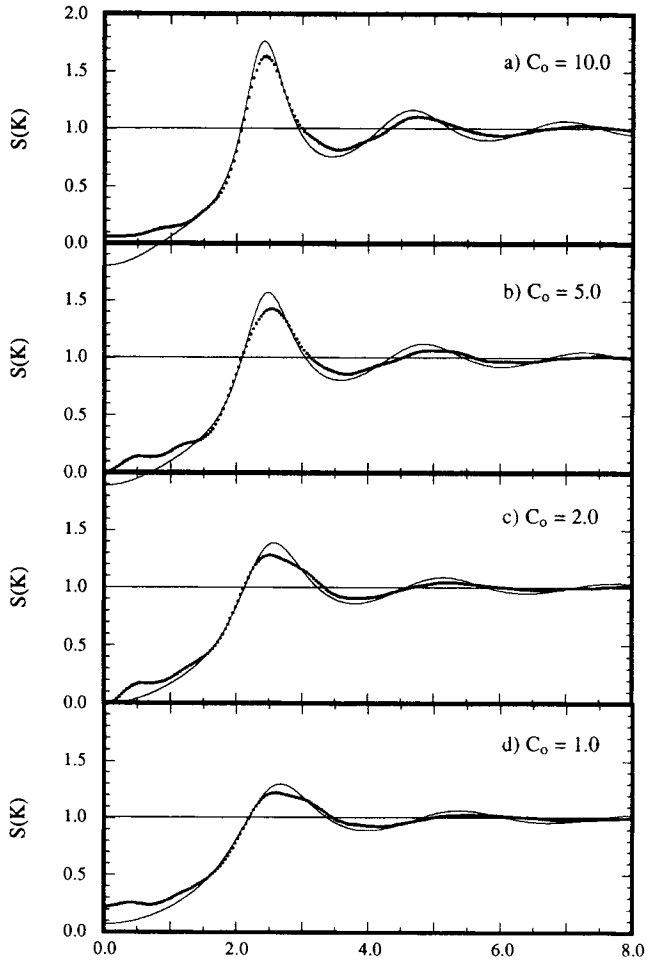

Figure 4. Static structure factors calculated for $h_o = 1.333$ and $\phi = 0.149$ at the indicated C_o values, from Brownian dynamics results (■ ■ ■) and for equivalent hard-sphere systems (——).

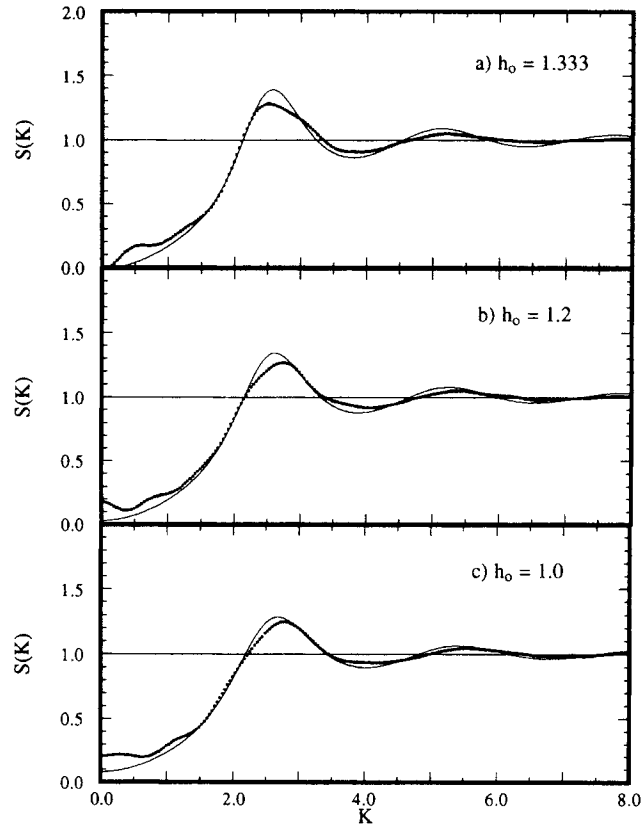

Figure 5. Static structure factors calculated for $C_o = 2.0$ and $\phi = 0.149$ at the indicated h_o values, from Brownian dynamics results (■ ■ ■) and for equivalent hard-sphere systems (——).

context of subsequent comparisons to experiment is the consistency of the primary peak locations of the steric and equivalent hard-sphere $S(K)$ curves.

Comparison to Experimental System

Markovic and coworkers (1986) conducted small-angle neutron scattering (SANS) experiments on 0.01-μm monodisperse poly(methyl methacrylate) (PMMA) particles from which they obtained static structure factors at several particle concentrations. The particles were stabilized in dodecane with poly (12-hydroxystearic acid) terminally attached through chemical bonds. From their results, they characterized the particle interactions using a potential of the Yukawa form. Here, we attempt to replicate the microstructure of the PMMA experimental system with Brownian dynamics and the MWC potential to evaluate the suitability of the MWC potential and to understand the interactions in this system.

To compare the experimental results with Brownian dynamics simulations, several parameters must be determined, including the core particle radius a; the concentration of particles (either number density N_p or core particle volume fraction ϕ); stabilizer thickness of a free particle, $h_o/2$; and the magnitude parameter of the potential, C_o. Three of the four parameters are available *a priori* from auxiliary measurements made by Markovic and coworkers (1986), and the fourth, C_o, is considered an adjustable parameter. (Possible sources of error in these parameter measurements are discussed subsequently.) If the MWC potential accurately models the particle interactions in this system, a single value of C_o should reproduce the experimental $S(K)$ at all concentrations. The core particle radius and stabilizer thickness were determined by Markovic and coworkers to be 150 Å and 100 Å, respectively, which corresponds to $h_o = 1.333$.

Markovic and coworkers (1986) determined the particle concentration by drying a sample of known weight, measuring the weight of the dried particles and stabilizer, and calculating the volume fraction of the particle plus stabilizer (ϕ_2). Their analysis assumed an average density for particle plus stabilizer. The volume fractions calculated in this way correspond to the outer particle radius, so the relationship between the number density N_p and the measured volume fraction is

$$\phi_2 = \frac{4}{3}\pi\left(1+\frac{h_o}{2}\right)^3 N_p \tag{21}$$

Markovic and coworkers presented $S(K)$ data at the volume fractions and corresponding number densities in Table 4, where ϕ follows directly from Eq. 11.

Table 4. PMMA Particle Concentrations Used in SANS Experiments (Markovic et al., 1986) and Brownian Dynamics Simulations

ϕ_2	N_p	ϕ
0.42	0.0217	0.0907
0.36	0.0186	0.0777
0.28	0.0144	0.0605
0.23	0.0119	0.0497

Before SANS and Brownian dynamics results are compared, the physically correct order of magnitude of C_o is sought. Cairns and coworkers (1981) measured osmotic pressures in suspensions of PMMA particles that were five times larger than the particles used in the SANS experiments, but with the same solvent and stabilizing polymer. They also conducted Monte Carlo and cell model (van Megen and Snook, 1978) calculations of the osmotic pressure using the potential (Ottewill and Walker, 1968)

$$U_s(s) = C_s\left(\frac{h_o}{2} - \frac{s}{2}\right)^2\left(3 + h_o + \frac{s}{2}\right) \qquad (22)$$

In general, C_s depends on interaction parameters, polymer concentration, and the particle radius. Cairns and coworkers (1981) found reasonable agreement between the experimental measurements and the theoretical predictions for $C_s = 7 \times 10^4$, which becomes $C_s \approx 500$ when scaled for the smaller particles in the SANS experiments. This gives only a rough estimate of C_o, because the shape of the potential in Eq. 22 is much softer at small separations than the MWC potential.

A straightforward way of obtaining the potential of interaction is from direct force measurements between two crossed cylinders at small separations (Israelachvili and Adams, 1978). Using the MWC potential, Milner (1988) was successful in quantitatively predicting direct-force measurements of a system of polystyrene chains ($M_w = 1.41 \times 10^5$) terminally attached to mica cylinders in toluene. The parameters of the potential were determined from osmotic pressure and radius of gyration measurements, which resulted in $C_o = 300$. This system is very different from the PMMA particles with poly (12-hydroxystearic acid) 'brushes' that were used in the SANS measurements, but it does indicate the expected order of magnitude of C_o. Although most of the physical information required to determine C_o for the SANS system is not known, the C_o of the polystyrene system can be adjusted for the difference in chain length to give $C_o \approx 50$. Therefore, the C_o for the SANS system is likely to be greater than 10, but less than 1,000.

Brownian dynamics simulations were conducted with 256 particles at the concentrations in Table 4 with $h_o = 1.333$, $N_c = 20{,}000$ and $\Delta t = 0.0005$. Results are presented for two values of C_o (20 and 200) at the highest and lowest concentrations, which indicate the ability of the MWC potential to reproduce the SANS data using C_o as the only adjustable parameter. Figures 6 and 7 compare the computed structure factors $S(K)$ with those reported by Markovic and coworkers (1986) for their experimental systems at the highest and lowest concentrations; the intermediate concentrations show behavior between these extremes. The experimental peak heights are

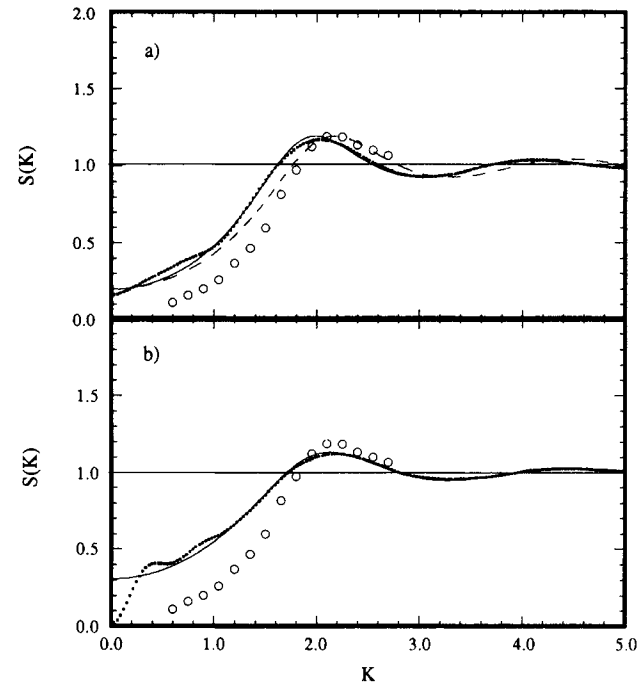

Figure 6. Static structure factors from Brownian dynamics simulations (■ ■ ■) with $h_o = 1.333$, $\phi = 0.0497$, and $C_o = 200$ (a) and $C_o = 20$ (b), from Markovic and coworkers (1986) for $\phi_2 = 0.23$ (○), for equivalent hard spheres of the Brownian dynamics systems (——), and for the estimated equivalent hard-sphere system of the experimental system (— —).

consistently predicted by the MWC potential for a single value of $C_o = 200$ (Figures 6a and 7a). However, the peak positions do not coincide; the primary peak of the SANS data is to the left of the Brownian dynamics peak, and the gap widens as the concentration increases.

In addition to the SANS and Brownian dynamics results, curves are also included in Figures 6 and 7 for equivalent hard-sphere systems, which are based on the parameters and particle concentrations used in the Brownian dynamics simulations. A second set of hard-sphere curves is included in the figures for $C_o = 200$ (shown as dashed lines), which correspond to the same hard-sphere concentrations as the first set, but for different hard-sphere radii. These will be discussed below. The first set of hard-sphere results show excellent agreement with the Brownian dynamics results except at low K, and agreement improves as C_o increases because the potential becomes more hard-sphere-like as it becomes stronger. The primary peak heights of the Brownian dynamics, SANS, and hard-sphere $S(K)$ curves correspond at $C_o = 200$.

The topography of the hard-sphere $g(r)$ and $S(K)$ curves is established by the single parameter ϕ_{hs}, the hard-sphere volume fraction. The hard-sphere radius scales the domains of $g(r)$ and $S(K)$, but does not affect the height and depth of the maxima and minima. Therefore, only one hard-sphere volume fraction will produce a given primary peak height in $S(K)$. If it is assumed that the primary peak height of the SANS $S(K)$ data corresponds to the peak height of the true unknown equivalent hard-sphere system, then matching peak

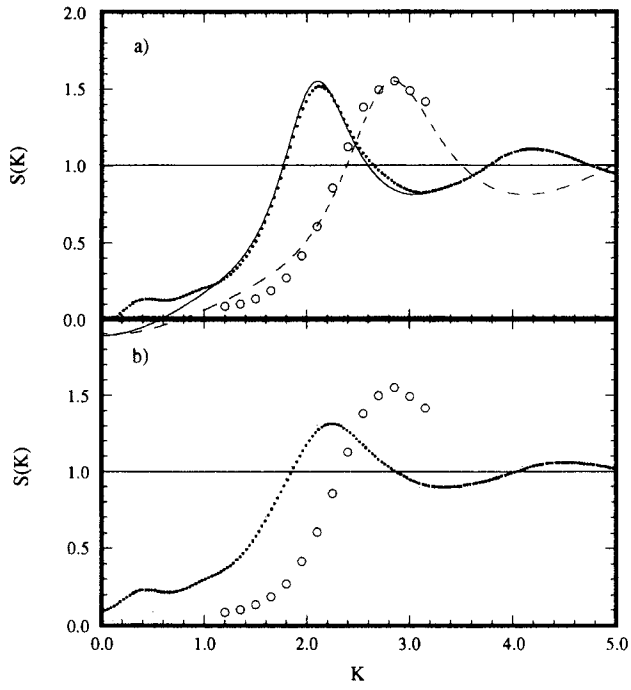

Figure 7. Static structure factors from Brownian dynamics simulations (■ ■ ■) with $h_o = 1.333$, $\phi = 0.0907$, and $C_o = 200$ (a) and $C_o = 20$ (b), from Markovic and coworkers (1986) for $\phi_2 = 0.42$ (○), for equivalent hard spheres of the Brownian dynamics systems (——), and for the estimated equivalent hard-sphere system of the experimental system (— —).

heights will give the equivalent hard-sphere concentration ϕ^e_{hs} of the experimental system at each of the four concentrations, and matching primary peak positions will give the equivalent hard-sphere radius a^e_{hs}. The equivalent hard spheres of the MWC potential with $C_o = 200$ give primary peaks in $S(K)$ that correspond in height to the SANS data, implying that those hard-sphere concentrations correspond closely to the actual equivalent hard-sphere concentrations of the experimental systems. The equivalent radius of the hard-sphere system could then be identified by scaling the abscissa to match the peak positions of the SANS data. Table 5 gives the equivalent hard-sphere attributes obtained by this procedure for the experimental systems. The region to the left of the primary peaks of the experimental $S(K)$ curves are poorly fit at the low concentrations by the hard-sphere theory (Figure 6a), but the fit is reasonably good at the higher concentrations (Figure 7a).

The hard-sphere radius estimates in Table 5 show a strong dependence on particle concentration; the radius increases by 20% between the highest and lowest concentrations. This is inconsistent with the premise of the Barker and Henderson (1967) theory, which assumes that the equivalent hard-sphere radius is characteristic of the potential only (in contrast to, for example, the perturbation theory of Andersen et al., 1971). A concentration-dependent equivalent hard-sphere radius is consistent with the physical picture of compression and densification of the polymer brushes.

Table 5. Estimated Effective Hard-Sphere Attributes of the Experimental SANS Systems Based on Static Structure Factors

ϕ_2	a^e_{hs}	ϕ^e_{hs}
0.42	1.116	0.2232
0.36	1.227	0.1440
0.28	1.340	0.0860
0.23	1.377	0.0650

Discussion

Agreement between the experimental $S(K)$ and Brownian dynamics curves is moderately good at low concentration at a consistent value of C_o. The discrepancy at large ϕ is appreciable, however, and cannot be corrected by adjusting C_o; this point is illustrated by the changes in $S(K)$ as C_o is increased from 20 to 200. The question remains as to whether the disparities are attributable to the potential model or caused by inaccuracies in the characterization or interpretation of the data. Certainly, the experimental results show the particles approaching much more closely than permitted by the model potential in the simulations. Therefore, either the model potential overestimates the repulsive force or there is a problem in interpretation of the experimental data, or both. Several possibilities are considered in this regard.

The MWC steric model assumes that chains do not interpenetrate as two particles approach; rather, the chains compress. Napper (1983) argues that extremely high surface coverages are required before interpenetration is inhibited, because in a good solvent, even at high coverage, the segment concentration is low at the extremity of the brushes. This implies that the MWC potential overestimates the loss of free energy and is too hard, particularly at low concentrations where the stabilizer overlap is modest.

Other obvious limitations of the MWC potential are failure to diverge until the surface separation goes to zero, which neglects the finite volume of polymer chains, and neglect of a "foot" in the segment density profile predicted by the Scheutjens and Fleer mean field equations at the outer extremity of the brushes (Cosgrove et al., 1987; Milner, 1990). These are unlikely to be major effects in the situation analyzed here. Neglect of curvature under conditions where the ratio of stabilizer thickness to particle radius is of order unity is likely to have some effect; here, $h_o/2 = 0.667$, and the splaying of the polymer brushes would certainly soften the potential.

The two most important experimental parameters are the core particle radius, which is the characteristic length used throughout the Brownian dynamics formulation, and the particle concentration, which has a strong influence on the radial distribution function and static structure factor obtained from Brownian dynamics.

The particle radius and stabilizer thickness are based on the interpretation of intraparticle scattering measured at low concentration (Markovic et al., 1986). The data were fit to a theoretical form for concentric spheres, which assumes that both the core and shell have constant scattering densities. This neglects the scattering profile in the stabilizer layer. If the homogeneous-shell interpretation represents an average scattering density with an effective shell thickness that is smaller than the true shell thickness, then the steric interaction in the physical system is actually longer range than $h_o = 1.333$.

It is difficult to reconcile the reported core radius of 150 Å

with the experimental structure factor data of Marcovic and coworkers (1986). When Fourier transformed to obtain the radial distribution function, these data show core separations approaching zero [nonzero $g(r)$ as $r \to 2$] as the volume fraction increases. Electron micrographs of carbon replicas of the core particle plus (dry) stabilizer indicate an average radius of 185 Å, with a coefficient of variation of 8%; this implies that the minimum separation ever achievable for particles with a core of 150 Å is 70 Å, requiring $g(r)$ to remain equal to zero at least to $r = 2.47$. Other uncertainties in the analysis of the scattering data, including the method used to account for intraparticle scattering and neglect of multiple scattering and particle deformability, are unlikely to be important in the current context.

The particle number density was obtained by Marcovic and coworkers from mass difference measurements by assuming an average density for the core particle plus stabilizer, with the stabilizer thickness determined from dilute SANS measurements. This procedure is quite sensitive to uncertainties in the stabilizer thickness because of the cubic dependence in Eq. 21. In addition, the interpretation is based on a solvated particle radius, while the concentration measurement utilizes dry particles. Hence, the reported particle concentrations could contain systematic errors which cannot be evaluated with the available information.

Effects of Hamaker Attractive Forces

Brownian dynamics simulations were performed with both steric and Hamaker forces for several values of C_o at two particle concentrations, with $h_o = 1.333$. The additional dimensionless parameter A was assigned the value 1.2146, which is the same value used by Cairns et al. (1981) in their Monte Carlo and cell model calculations. This value is consistent with general guidelines for Hamaker forces in organic systems (Russel, 1987). Detailed results are contained in TeGrotenhuis (1991). The most notable effect of Hamaker forces is the loss of stability in the system when the steric forces are not strong enough; instability is manifested in the simulations as catastrophic particle overlap and loss of meaningful results due to the absence of a short-range hard core in the potential of interaction. Aggregation would occur if a hard core was implemented. When $C_o \leq 5.0$, the suspension is unstable for $\phi > 0.149$, and when $C_o \leq 8.0$, the system is unstable for $\phi > 0.224$. This lends some credibility for estimating $10 \leq C_o \leq 1{,}000$, but is inconclusive because of the limitations of the MWC potential noted previously. The osmotic pressure is relatively unaffected at the concentrations studied, which are generally higher than concentrations used in the simulations of Figures 2 through 7. Inclusion of Hamaker forces cannot account for the discrepancies between the experimental and Brownian dynamics results that were observed previously.

Self-Diffusion

Hydrodynamic interactions were included in simulations used to calculate the self-diffusion coefficients from the mean-square displacement curve. The hydrodynamic interactions do not account for the stabilizer layer, but assume that the continuous fluid extends at constant viscosity to the surface of the core particles. The alternate approach of rescaling the hydrodynamics with an additional length scale that reflects the effective hydrodynamic radius is not possible, since two particles can approach within a distance that is less than twice the hydrodynamic radius and this is interpreted by the hydrodynamic calculations as particle overlap. A correct implementation of hydrodynamics for sterically stabilized particles would be to specify a hydrodynamic radius that is larger than the core particle radius and then allow deformation of the hydrodynamic particle, but this was not attempted.

A series of simulations was conducted without hydrodynamics at $\phi = 0.149$ with $N = 108$ and 256 for time steps ranging from 0.00005 to 0.0005 to explore the effects of system size and time step on calculated equilibrium properties and on the self-diffusion coefficient (TeGrotenhuis, 1990). The results indicated systematic error in D_s/D_o; self-diffusion decreased as Δt decreased and as the system size decreased, but the changes were less than 10%.

Self-diffusion coefficients were calculated at several volume fractions with $C_o = 20.0$ and $h_o = 1.333$, with and without hydrodynamic interactions. As expected, equilibrium properties were insensitive to the presence or absence of hydrodynamic interactions. The calculated self-diffusion coefficients are shown in Figure 8. There is no trend to the differences between points calculated with and without hydrodynamic interactions. The scatter in the points at lower concentrations is consistent with our previous discussion (TeGrotenhuis et al., 1989) that the error in calculated self-diffusion coefficients increases with decreasing concentration. Self-diffusion is a monotonically decreasing function of concentration for a purely repulsive potential, so any increases in D_s as concentration increases must be due to statistical error.

The theory of self-diffusion of hard spheres in a vacuum (Ackerson and Fleishman, 1982; Hanna et al., 1982; Ohtsuki and Okano, 1982a) gives the linear result

$$\frac{D_s^{hs}}{D_o} = 1 - 2\phi_{hs} \tag{23}$$

in the limit of low volume fraction. Batchelor (1983) and Yoshida (1983) both incorporated hydrodynamic interactions for monodisperse suspensions and obtained small corrections;

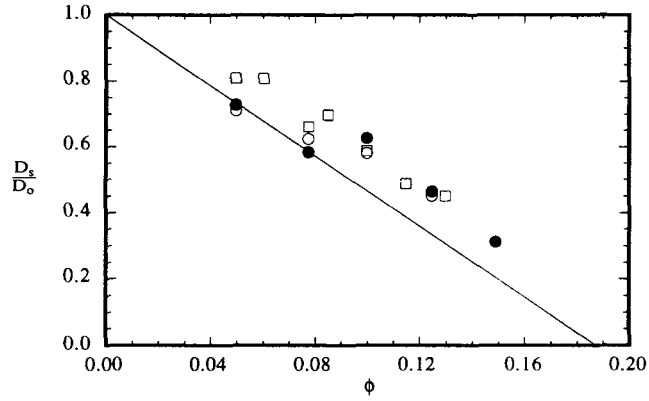

Figure 8. Self-diffusion coefficient dependence on volume fraction, without hydrodynamic interactions for $N = 256$ (□), without hydrodynamic interactions for $N = 108$ (○), with hydrodynamic interactions for $N = 108$ (●), and linear theory for equivalent hard spheres (——).

Batchelor found 2.10 as the linear coefficient, indicating hydrodynamic interactions retard self-diffusion, while Yoshida obtained 1.996, indicating slightly enhanced self-diffusion. In both cases, the effects of hydrodynamic interactions are an order of magnitude lower than the excluded volume effects, which is consistent with the results obtained here for sterically stabilized particles. For $C_o = 20.0$ and $h_o = 1.333$, the effective hard-sphere radius is $a_{hs} = 1.3872$, which when substituted into Eqs. 19 and 23 gives

$$\frac{D_s}{D_o} = 1 - 5.339\phi \tag{24}$$

A line corresponding to Eq. 24 is included in Figure 8. The hard-sphere theory lies below the best-fit line through the data, which is not shown. The disparity could be due to higher order terms, which must eventually increase the self-diffusion coefficient to prevent the theory from predicting negative diffusion coefficients. It is also possible that the limiting slopes of the mean-square displacement curves at long times were not achieved, leading to an overprediction of the self-diffusion coefficient (Ohtsuki, 1982b; Hess and Klein, 1981).

It is worth noting that the equilibrium MWC potential was used to calculate a transport property, which inherently involves a dynamic process. This inconsistency is also present in other types of colloidal interactions, including electrostatic, but is likely to be more important here where relaxation processes are longer.

Conclusions

Brownian dynamics is a powerful tool for establishing both equilibrium and transport properties of model colloidal suspensions. The simulations reported here for colloids interacting through the short-range steric potential of Milner, Witten, and Cates (1988) point to the deficiencies in the theory, notably the extent of "softness" of the potential, and they raise questions about the SANS experimental approach to structure determination in systems of this type. It is clear that unambiguous determination of the critical parameters for simulation is essential for a proper comparison between experimental structure measurements and Brownian dynamics simulations. It can be concluded that systems following the MWC potential can be approximated by equivalent hard spheres, particularly as the steric interaction becomes stronger, except for the calculation of short-range structure. The hard-sphere approximation, as evaluated using osmotic pressure calculations, becomes poorer as the concentration approaches the hard-sphere phase transition. Hamaker forces have little effect on the calculated equilibrium properties, but their inclusion can lead to loss of suspension stability when the steric potential is too soft. Finally, the change in self-diffusion coefficient with concentration is predominately due to excluded-volume effects in the concentration and steric potential range studied; the effect of hydrodynamic interaction is smaller by an order of magnitude.

Acknowledgment

This work was supported by the Director, Office of Energy Research, Office of Basic Energy Sciences, Materials Science Division of the U.S. Department of Energy under Contract No. DE-AC03-76SF00098.

Notation

a = radius of colloidal particles
a_{hs} = equivalent hard sphere radius
$\mathfrak{a}$ = size of monomer unit in a freely-jointed chain of equivalent length
A = Hamaker force constant
$\boldsymbol{A}$ = N-particle Brownian force vector
C_o = dimensionless magnitude parameter of Milner, Witten and Cates steric potential
C_s = dimensionless magnitude parameter of steric potential used by Ottewill and Walker (1968)
D_o = free-particle diffusion coefficient
D_s = self-diffusion coefficient
$D_{s,L}$ = long-time self-diffusion coefficient
D_s^{hs} = self-diffusion coefficient of equivalent hard spheres
$\boldsymbol{F}$ = N-particle net interparticle force vector
$\boldsymbol{F}_i$ = net interparticle force on particle i
$\boldsymbol{F}_{ij}$ = interparticle pair force vector from particle j to particle i
$g(r)$ = radial distribution function
h^* = equilibrium thickness of polymer chains attached to a single flat plate
h_o = dimensionless distance parameter of Milner, Witten and Cates steric potential
$\boldsymbol{I}$ = identity matrix
k = Boltzmann's constant
K = magnitude of the wavevector
L_b = cubic edge length of the system
m = number of time steps between adjacent points in the calculated mean square displacement curve
$\boldsymbol{m}$ = inertial tensor for the system of particles
N = number of particles in the system
N_c = number of particle configurations sampled when calculating average properties
N_f = polymerization index of attached polymer chains
N_o = number of starting times used in run-time averaging
N_p = particle number density of simulated suspension
P = osmotic pressure of the suspension
P_{CS} = osmotic pressure of hard sphere system calculated from Carnahan-Starling equation of state (1970)
r = center-to-center particle separation
r_{ij} = center-to-center separation of particles i and j
$\boldsymbol{r}_{ij}$ = vector from the center of particle j to the center of particle i
$\boldsymbol{r}_j(t)$ = position vector of particle j at time t
$\boldsymbol{R}$ = hydrodynamic resistance matrix
$\boldsymbol{R}_\infty$ = Stokes drag contribution to the hydrodynamic resistance matrix
s = surface-to-surface separation of two colloidal particles
$S(K)$ = static structure factor
t = time
t_e = length of previous simulations that were run at the same conditions to allow the system to relax to equilibrium
t_j^o = jth starting time used in run-time averaging
T = temperature
U_H = Hamaker interparticle pair potential
U_s = steric interparticle pair potential
$U(r)$ = interparticle pair potential
$\boldsymbol{v}$ = $6N$ vector of translational and angular velocities for N particles
w = excluded volume parameter in Milner, Witten and Cates steric potential
$\Delta r(t)$ = particle displacement in time t
Δt = time step of numerical integration of Langevin equation

Greek letters

δ = dirac delta function
μ = viscosity of suspending fluid
σ = surface coverage of polymer chains attached to a surface (chains/area)
ϕ = volume fraction of particles in the simulated suspension
ϕ_{hs} = equivalent hard sphere volume fraction
ϕ_2 = volume fraction of particles plus stabilizer layer for sterically stabilized particles
χ = Flory chi parameter

Literature Cited

Ackerson, B. J., and L. Fleishman, "Correlations for Dilute Hard Core Suspensions," *J. Chem. Phys.*, **76**, 2675 (1982).

Allen, M. P., and D. J. Tildesley, *Computer Simulation of Liquids*, Clarendon Press, Oxford (1987).

Andersen, H. C., J. D. Weeks, and D. Chandler, "Relationship Between the Hard-Sphere Fluid and Fluids with Realistic Repulsive Forces," *Phys. Rev. A*, **4**(4), 1597 (1971).

Barker, J. A., and D. Henderson, "Theories of Liquids," *Annual Rev. Phys. Chem.*, **23**, 439 (1972).

Barker, J. A., and D. Henderson, "Perturbation Theory and Equation of State for Fluids: II. A Successful Theory of Liquids," *J. Chem. Phys.*, **47**(11), 4714 (1967).

Batchelor, G. K., "Diffusion in a Dilute Polydisperse System of Interacting Spheres," *J. Fluid Mech.*, **131**, 155 (1983); "Corrigendum," *J. Fluid Mech.*, **137**, 467 (1983).

Bossis, G., B. Quentrec, and J. P. Boon, "Brownian Dynamics and the Fluctuation-Dissipation Theorem," *Mol. Phys.*, **45**(1), 191 (1982).

Brenner, H., "The Stokes Resistance of an Arbitrary Particle: II. An Extension," *Chem. Eng. Sci.*, **19**, 599 (1964).

Cairns, R. J. R., W. van Megen, and R. H. Ottewill, "A Comparison between Theoretically Computed and Experimentally Measured Pressures for Interacting Sterically Stabilized Particles," *J. Colloid and Interface Sci.*, **79**(2), 511 (1981).

Carnahan, N. E., and K. E. Starling, "Equation of State for Nonattracting Rigid Spheres," *J. Chem. Phys.*, **51**, 635 (1969); "Thermodynamic Properties of a Rigid-Sphere Fluid," **53**, 600 (1970).

Chandler, D., *Introduction to Modern Statistical Mechanics*, Oxford University Press, New York (1987).

Chandrasekhar, S., "Stochastic Problems in Physics and Astronomy," *Rev. Mod. Phys.*, **15**, 1 (1943).

Ciccotti, G., and J.-P. Ryckaert, "On the Derivation of the Generalized Langevin Equation for Interacting Brownian Particles," *J. Stat. Phys.*, **26**(1), 73 (1981).

Cosgrove, T., T. Heath, B. van Lent, F. Leermakers, and J. Scheutjens, "Configuration of Terminally Attached Chains at the Solid/Solvent Interface: Self-Consistent Field Theory and a Monte Carlo Model," *Macromol.*, **20**, 1692 (1987).

Dahlquist, G., and A. Bjorck, *Numerical Methods*, Prentice-Hall, Englewood Cliffs, NJ, p. 453 (1974).

de Gennes, P. G., *Scaling Concepts in Polymer Physics*, Cornell University Press, Ithaca (1979).

Derjaguin, V. B., "Untersuchungen uber die Reibung und Adhasion: IV. Theorie des Anhaftens kleiner Teilchen," *Kolloid-Z.*, **69**, 155 (1934).

Deutch, J. M., and I. Oppenheim, "Molecular Theory of Brownian Motion for Several Particles," *J. Chem. Phys.*, **54**(8), 3547 (1971).

Dickinson, E., "Statistical Mechanics of Colloidal Suspensions," *Specialist Periodical Reports, Colloid Science*, Vol. 4, D. H. Everett, ed., The Royal Soc. Chem., London, U.K., p. 150 (1983).

Durlofsky, L., J. F. Brady, and G. Bossis, "Dynamic Simulation of Hydrodynamically Interacting Particles," *J. Fluid Mech.*, **180**, 21 (1987).

Ermak, D. L., and J. A. McCammon, "Brownian Dynamics with Hydrodynamic Interactions," *J. Chem. Phys.*, **69**(4), 1352 (1978).

Hamaker, H. C., "The London-van der Waals Attraction between Spherical Particles," *Physica*, **4**(10), 1058 (1937).

Hanna, S., W. Hess, and R. Klein, "Self-Diffusion of Spherical Brownian Particles with Hard Core Interactions," *Physica*, **111A**, 181 (1982).

Hess, W., and R. Klein, "Dynamical Properties of Colloidal Systems: III. Collective and Self-Diffusion of Interacting Charged Particles," *Physica*, **105A**, 552 (1981).

Hirschfelder, J. O., C. F. Curtis, and R. B. Bird, *Molecular Theory of Gases and Liquids*, Wiley, New York (1954).

Israelachvili, J. N., and G. E. Adams, "Measurement of Forces Between Two Mica Surfaces in Aqueous Electrolyte Solutions in the Range 0–100 nm," *J. Chem. Soc., Faraday Trans.*, **74**, 975 (1978).

Langevin, P., "Theory of Brownian Movement," *Compt. Rend.*, **146**, 530 (1908).

Markovic, I., R. H. Ottewill, S. M. Underwood, and T. F. Tadros, "Interactions in Concentrated Nonaqueous Polymer Latices," *Langmuir*, **2**(5), 625 (1986).

Marqusee, J. A., and J. M. Deutch, "Concentration Dependence of the Self-Diffusion Coefficient," *J. Chem. Phys.*, **73**(10), 5396 (1980).

Milner, S. T., T. A. Witten, and M. E. Cates, "Theory of Grafted Polymer Brush," *Macromol.*, **21**, 2610 (1988).

Milner, S. T., "Compressing Polymer Brushes: a Quantitative Comparison of Theory and Experiment," *Europhys. Lett.*, **7**(8), 695 (1988).

Milner, S. T., and T. A. Witten, "Bending Moduli of Polymeric Surfactant Interfaces," *J. Phys. (France)*, **49**, 1951 (1988).

Milner, S. T., "Strong-Stretching and Scheutjens-Fleer Descriptions of Grafted Polymer Brushes," *J. Chem. Soc., Faraday Trans.*, **86**(9), 1349 (1990).

Napper, D. H., *Polymeric Stabilization of Colloidal Dispersions*, Academic Press, London (1983).

Ohtsuki, T., and K. Okano, "Diffusion Coefficients of Interacting Brownian Particles," *J. Chem. Phys.*, **77**, 1443 (1982a).

Ohtsuki, T., "Dynamical Properties of Strongly Interacting Brownian Particles," *Physica*, **110A**, 606 (1982b).

Ottewill, R. H., and T. Walker, "The Influence of Non-Ionic Surface Active Agents on the Stability of Polystyrene Latex Dispersions," *Kolloid-Z. Z. Polymere*, **227**, 108 (1968).

Overbeek, J. Th. G., "Interparticle Forces in Colloid Science," *Powder Tech.*, **37**, 195 (1984).

Percus, J. K., and G. J. Yevick, "Analysis of Classical Statistical Mechanics by Means of Collective Coordinates," *Phys. Rev.*, **110**, 1 (1958).

Perram, J. W., "Hard Sphere Correlation Functions in the Percus-Yevick Approximation," *Molec. Phys.*, **30**(5), 1505 (1975).

Press, W. H., B. P. Flannery, S. A. Teukolsky, and W. T. Vetterling, *Numerical Recipes: The Art of Scientific Computing*, Cambridge University Press, New York (1986).

Russel, W. B., *The Dynamics of Colloidal Systems*, University of Wisconsin Press, Madison (1987).

Spiegal, M. R., *Probability and Statistics*, McGraw-Hill, New York (1975).

TeGrotenhuis, W. E., C. J. Radke, and M. M. Denn, "Self-Diffusion in Electrostatically Stabilized Colloidal Suspensions using Brownian Dynamics," *Mol. Sim.*, **2**, 3 (1989).

TeGrotenhuis, W. E., "Brownian Dynamics of Colloidal Suspensions," PhD Diss., Univ. of California at Berkeley (1990).

Throop, G. J., and R. J. Bearman, "Numerical Solutions of the Percus-Yevick Equation for the Hard-Sphere Potential," *J. Chem. Phys.*, **42**(7), 2408 (1965).

van Gunsteren, W. F., and H. J. C. Berendsen, "On the Fluctuation-Dissipation Theorem for Interacting Brownian Particles," *Mol. Phys.*, **47**(3), 721 (1982).

van Megen, W., and I. Snook, "Statistical Mechanical Approach to Phase Transitions in Colloids," *Faraday Disc. Chem. Soc.*, **65** (Colloid Stability), 92 (1978).

Weeks, J. D., D. Chandler, and H. C. Andersen, "Role of Repulsive Forces in Determining the Equilibrium Structure of Simple Liquids," *J. Chem. Phys.*, **54**(12), 5237 (1971).

Yoshida, N., "Concentration Dependence of the Self-Diffusion Coefficient of Hard Spheres in Solution," *Chem. Phys. Lett.*, **101**, 555 (1983).

Manuscript received Oct. 21, 1992, and revision received July 23, 1993.